Ab initio calculations of the atomic and electronic structure of clean and hydrogenated diamond (110) surfaces

G. Kern and J. Hafner
Institut für Theoretische Physik and Center for Computational Materials Science, Technische Universität Wien, Wiedner Hauptstraße 8-10, A-1040 Wien, Austria
(Received 8 April 1997)

We present *ab initio* local-density-functional calculations of the electronic structure of clean and hydrogenated diamond (110) surfaces. The clean surface relaxes to a structure where the chains in the first two planes are straightened so that the interatomic distances are shortened and the bond angles are increased. Upon relaxation the surface remains flat and no dimerization occurs. The dangling bonds lead to surface states within the bulk gap. The surface is metallic, but with a very low density of states at the Fermi level. After the deposition of a monolayer of hydrogen, which saturates all dangling bonds, the surface relaxes back to an almost bulk-terminated structure. The occupied surface states are removed from the gap and the surface becomes semiconducting. We also compare the C(110) surface with the other two low-index diamond surfaces. [S0163-1829(97)02831-2]

I. INTRODUCTION

The fact that diamond is a very promising material for future applications stimulated many research efforts. The development of chemical vapor deposition (CVD) processes for diamond growth has further increased the interest in the structural and electronic properties of the low-index faces of diamond. As we have already studied the diamond (100) (Refs. 1–3) and the diamond (111) (Refs. 4–6) surfaces, we now present our results for the diamond (110) surface. C(110) is the least studied surface among the low-index faces of diamond. The C(110) surface is not only important for the growth of (110) surfaces. At steps on (111) and (100) surfaces facets with (110) orientation appear and play an important role in the model of layer-by-layer growth.[7] For these reasons, an understanding of the structural and electronic properties of the C(110) surface is important for an improvement of the quality and growth rate of CVD processes.

Lurie and Wilson[8] examined the C(110) surface with low-energy electron diffraction (LEED) and found a (1×1) diffraction pattern. Unlike the (111) and (100) surfaces there were no changes after annealing of the surface. Thus a reconstruction can be excluded by LEED. Pate[9] showed with photon-stimulated ion desorption that heating over 1300 K removes most of the hydrogen from the surface. Photoemission experiments by Pepper[10] find changes in the electronic structure after annealing of the surface. He associated this with the desorption of hydrogen. McGonigal *et al.*[11] studied the C(110) surface with infrared spectroscopy and found a single frequency for the C-H stretching mode. They concluded that the hydrogen saturated C(110) surface is monohydride terminated. They also showed that atomic hydrogen is needed to saturate the dangling bonds of the clean surface. For molecular H_2 they found no changes in their spectra. Recent ultraviolet photoelectron spectroscopy (UPS) experiments from Francz *et al.*[12] showed an increase of electronic states around 3 and 13 eV below the valence-band maximum (VBM) after annealing of the C(110) surface. Nemanich, Baumann, and van der Weide[13] demonstrated that hydrogen termination can introduce a negative electron affinity on the C(110) surface.

Davidson and Pickett[14] studied the (110) surface using a semiempirical tight-binding method. They predicted dimerized clean and hydrogenated surfaces. With a non-self-consistent *ab initio* approach, Alfonso, Drabold, and Ulloa[15] proposed a symmetric but buckled clean, and a flat hydrogenated (110) surface. Due to these geometric differences they also obtained different results for the electronic structure. In this paper we examine the structural and electronic properties of the clean and hydrogen-covered diamond (110) surfaces using self-consistent *ab initio* local-density-functional (LDF) techniques.

II. THEORY

For our calculations we used the Vienna *ab initio* simulation package (VASP),[16,17] which is based on the following principles:

(1) We use the finite-temperature version of LDF theory[18] developed by Mermin,[19] with the exchange-correlation functional given by Ceperley and Alder as parametrized by Perdew and Zunger.[20] Finite-temperature LDF theory introduces a smearing of the one-electron levels and helps to solve convergence problems arising from using a small set of $\vec{k}$ points for Brillouin-zone integrations, the use of fractional occupancies eliminates all instabilities that can arise from a crossing of levels in the vicinity of the Fermi energy. The variational quantity in finite-temperature LDF theory is the electronic free energy.

(2) The solution of the generalized Kohn-Sham equations is performed using an efficient matrix-diagonalization routine based on a sequential band-by-band residual minimization method (RMM) for the one-electron energies.[17,21]

(3) In the doubly iterative RMM method it is essential to use an efficient charge-density mixing routine to avoid charge-sloshing problems. We use an improved Pulay mixing for calculating the new charge-density and potential.[22]

We have found that the sequential band-by-band algorithm combined with an efficient mixing algorithm is considerably faster than conjugate-gradient (CG) algorithms attempting a direct minimization of the energy by treating all bands simultaneously.[17]

(4) The optimization of the atomic geometry is performed via a conjugate-gradient minimization of the total energy with respect to the atomic coordinates.

(5) After moving the atoms, the new charge densities are estimated by extrapolating the results of the last steps.

(6) The calculation has been performed using fully nonlocal optimized ultrasoft pseudopotentials.[23,24] The nonlocal contributions are calculated in real space, using the optimized projectors introduced by King-Smith, Payne, and Lin.[25] Details of the pseudopotentials with a cutoff energy of $E_{\rm cut}=$ 270 eV are given in Refs. 4 and 26.

III. COMPUTATIONAL ASPECTS OF THE MODELING OF THE C(110) SURFACE

In our calculations we represented the C(110) surface by periodically repeated symmetric and asymmetric (second surface hydrogen terminated) slabs of varying thickness in a (2×1) surface cell. We found that for the geometrical relaxations a slab of 12 carbon layers is sufficient, but for accurate absolute energies a 16-layer slab is necessary (relative surface energies are converged to 1 meV with a 12-layer slab). Six layers were allowed to relax. This is enough because the fifth and the sixth layer practically retain their positions. The slabs are separated by a vacuum region of 6 layers, corresponding to 9 Å for the clean and 7 Å for the symmetric hydrogenated slab, respectively. Increasing the width of the vacuum to 10 layers leads to an increase in the total energy of only 12 meV, but no changes in relative surface energies or structural changes were observed.

For the Brillouin-zone integrations we used various grids of Monkhorst-Pack special points,[27] together with the Methfessel-Paxton technique for a smearing of the one-electron energies[28] within the finite-temperature LDF scheme. In the Methfessel-Paxton approach, the step function representing the Fermi-Dirac occupation probability is approximated by an expansion in terms of Hermite polynomials. In combination with a first-order approximation to the smearing function, a width of $\sigma=$ 0.1 eV has been determined as the optimal choice. For the structural relaxation a $4\times6\times1$ grid with 4 irreducible $\vec{k}$ points is sufficient. The surface energies are calculated using a $7\times11\times1$ grid with 24 irreducible $\vec{k}$ points and the linear tetrahedron method,[29] including the corrections proposed by Blöchl, Jepsen, and Andersen.[30] To get better results for the energies we turned off the real-space projection [see Sec. II, principle (6)]. These provisions reduce the error of the absolute energy due to the Brillouin-zone integration to $\leqslant$ 5 meV.

The symmetric and asymmetric slabs did not show differences in either the structural relaxations or the band structures. The difference in the relaxation energy of the clean surface is 4 meV. Hence we arrive at the following standard setting for the calculation of the total energy (with an estimated error in the absolute and relative surface energies of $\leqslant$ 20 and $\leqslant$ 5 meV, respectively) and equilibrium geometry of the surface: (2×1) surface cell, 16 layers in the slab (i.e., 32 atoms in the cells representing the clean surfaces, 36 for the hydrogenated surfaces), 6 layers are allowed to relax, 6 layers of vacuum separating the repeated slabs, $(4\times6\times1)$ Monkhorst-Pack grid, Methfessel-Paxton smearing of first order with $\sigma=$ 0.1 eV. The total energy and the electronic density of states were calculated with a $7\times11\times1$ grid and the linear tetrahedron method at fixed geometries.

IV. OPTIMIZATION OF THE SURFACE GEOMETRY

In the following we describe the changes in the surface geometry of the clean and the hydrogenated surfaces determined by an optimization of the atomic geometry in a (2×1) surface cell. We carefully checked for possible reconstructions proposed by other groups, i.e., dimerization of the surface bonds[14] or buckling of the surface.[15] In the bulk the interatomic distance is $d=1.529$ Å at the calculated equilibrium lattice constant of $a_0=3.531$ Å. The experimental value of the lattice constant is $a_0=3.567$ Å. This difference is due to the characteristic LDF error. To introduce no stress we used the theoretical lattice constant for our surface calculations.

A. Clean surface

For the clean bulk-terminated C(110) surface we calculate a cleavage energy of $E_{\rm surf}=$ 2.089 eV per atom. This is the lowest value of the three low-index faces. The other diamond surface with one dangling bond (1db) per atom, the 1db C(111) surface, has a 0.66 eV higher cleavage energy.[4]

Relaxing the slab lowers the surface energy by $E_{\rm rel}=-0.429$ eV per atom to $E_{\rm surf}=1.660$ eV per atom. Compared to the C(111) surface the relaxation energy is reduced by 0.15 eV. Upon relaxation, the surface layer moves inward by -0.17 Å, the first subsurface layer moves outward by 0.03 Å. The atoms of the first two layers move also in the [001] direction in such a way that the chains in the planes are straightened and the interatomic distances are shortened (see Table I). The resulting bond length in the first layer is 1.42 Å (-7% relative to the bulk value) and in the second layer 1.49 Å (-2.5%). The bond angles are increased to 123° and 114° in the surface and the subsurface layer, respectively. Hence the character of the bonds in the surface changes from sp^3 bonded diamond ($d=1.53$ Å, $\theta=109.5°$) to sp^2 bonded graphite ($d=1.43$ Å, $\theta=120°$). The bond lengths between the first and the second (the second and the third) layer are decreased (increased) by 0.06 Å (0.05 Å). All other relaxations are $\leqslant$ 0.01 Å. The relaxed C(110) surface is shown in Fig. 1(a).

We then tried to produce a (2×1) reconstruction by starting with dimerized and buckled surfaces and relaxed them to their ground state. We used also denser $\vec{k}$-point grids, some centered on the Γ point so that they contained grid points on the Brillouin-zone boundary. However, each surface relaxed back to the symmetric, flat (1×1) structure. This is in unison with the LEED experiments from Lurie and Wilson,[8] but in contrast to the calculations of Davidson and Pickett[14] and Alfonso, Drabold, and Ulloa.[15] The tight-binding calculation of Davidson and Pickett gave a dimerization of 0.8% in the surface layer and also dimerization in each layer down to the fifth between 0.5 and 0.7%. The fact that there should be an

TABLE I. Structural properties of the relaxed C(110) surfaces. d_{ij} is the bond length between the carbon atoms of the ith and jth layers, d_{H1} is the distance between the hydrogen and the carbon atom of the first layer. The value in parentheses is the change of the bond length relative to the bulk bond length of 1.529 Å. The angles θ_i refer to the bond angles between atoms of the ith layer (chain angle), while $\theta_{H1\hat{n}}$ is the angle between the H bond and the normal to the surface. Δx_i and Δz_i are the relaxations of the atomic positions in x ([001]) and z direction ([110]) of the ith layer, respectively.

	C(110)		C(110):H	
d_{11} (Å)	1.419	(−7.2%)	1.508	(−1.4%)
d_{12} (Å)	1.467	(−4.1%)	1.520	(−0.6%)
d_{22} (Å)	1.490	(−2.6%)	1.526	(−0.2%)
d_{23} (Å)	1.576	(+3.1%)	1.533	(+0.2%)
d_{33} (Å)	1.526	(−0.2%)	1.530	(+0.0%)
d_{34} (Å)	1.528	(−0.1%)	1.529	(−0.0%)
d_{H1} (Å)			1.106	
θ_1 (deg)	123.3		111.8	
θ_2 (deg)	113.8		109.8	
$\theta_{H1\hat{n}}$ (deg)			33.5	
Δx_1 (Å)	±0.10		±0.02	
Δz_1 (Å)	−0.17		−0.02	
Δx_2 (Å)	±0.03		±0.00	
Δz_2 (Å)	+0.03		+0.00	

almost constant dimerization in the first five layers is a little bit astonishing. The non-self-consistent calculations of Alfonso, Drabold, and Ulloa predict a strongly buckled ($\Delta z = 0.14$ Å) surface. We also note that the non-self-consistent calculation leads to a large value for the bulk bond length of 1.57 Å, in marked contrast to the well-known tendency of the LDF to underestimate rather than to overestimate the bond length and to the accurate prediction derived from our self-consistent calculations.

B. Hydrogenated surface

After the deposition of a monolayer of hydrogen, which saturates all dangling bonds, the surface relaxes back to an almost bulk-terminated structure. Compared to this structure, the atoms of the first layer move by 0.02 Å inward and by 0.02 Å in the [001] direction. All other relaxations relative

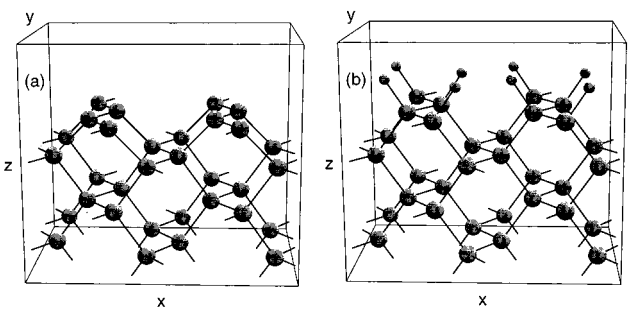

FIG. 1. Perspective views of the relaxed clean (a) and hydrogenated (b) C(110) surfaces. Carbon atoms: large spheres; hydrogen atoms: small spheres. The z axis is oriented along the [110] direction, the y axis along $[\bar{1}10]$, the x axis along [001].

TABLE II. Energetics of the clean and hydrogenated C(110) surfaces (in eV per surface site). E_{surf} refers to the absolute surface energy per atom. The surface energy is measured relative to the total energy of N C atoms in bulk diamond (N denotes the number of atoms in the slab). For the hydrogenated surface, the spin-polarized energy of the free hydrogen atoms has been taken into account. E_{rel} is the relaxation energy relative to the bulk-terminated surface. The adsorption energy E_{ad} measures the energy gained by adsorbing a free H atom on the clean, relaxed C(110) surface.

Structure	E_{surf}	E_{rel}	E_{ad}
C(110) ideal	2.089		
C(110) relaxed	1.660	−0.429	
C(110):H	−2.677	−4.765	−4.337

to the bulk-terminated surface are $\leqslant 0.005$ Å. The C–H bond length is 1.11 Å, the bond forms an angle of 33.5° with the surface normal. In the surface chain the bond length is increased from 1.43 Å on the clean relaxed surface to 1.51 Å by the hydrogenation. The bond angle decreases to 112°. Thus by saturating the dangling bonds with hydrogen, the surface is much more diamondlike than the clean relaxed surface. The bond length between the first and the second layer is $d_{12} = 1.52$ Å. All other C–C distances are within ±0.005 Å equal to the bulk interatomic distances (see Table I).

The surface energy $E_{surf} = -2.677$ eV per atom is 4.34 eV lower than the surface energy of the clean relaxed C(110) surface (see Table II). Because the adsorption energy $E_{ad} =$ 4.34 eV per atom is larger than the molecular binding energy per atom of the hydrogen molecule [$E(H_2) = 2.45$ eV/atom within the LDF], a dissociative adsorption of H_2 on the C(110) surface should be possible, unless there is a large barrier in the entrance channel.

V. ELECTRONIC PROPERTIES

For the determination of electronic surface states the eigenstates given in a plane-wave basis must be projected onto a local basis. This can be done by projecting the individual plane-wave components onto the spherical waves within the atomic spheres drawn around each atomic site. The radius of the spheres is chosen such that the sum of the local density of states reproduces the total density of states (slightly larger than the Wigner-Seitz radius). Details of the projection technique are described in the paper by Eichler, Hafner, Furthmüller, and Kresse.[31]

For the symmetric 16-layer slabs we define a surface state as a state whose intensity is concentrated to more than 70% on the first two layers on each side. For the hydrogenated surface the intensities of the hydrogen atoms are added to the surface carbon intensities. To visualize the degree of localization of a surface state we use three different degrees of shading to represent states that are localized to more than 70, 80, and 90% on the surface, darker shading corresponding to stronger localization (see Figs. 2 and 6). Calculations of the asymmetric slabs gave very similar results.

A. Clean surface

Figure 2 shows the dispersion relations of the electronic surface states for the clean relaxed C(110) surface. We

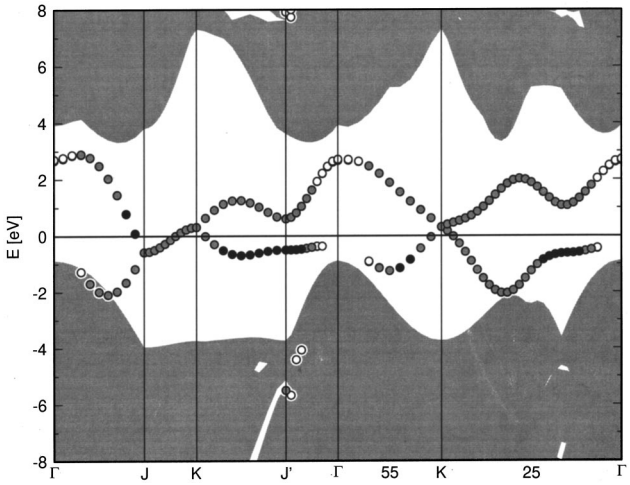

FIG. 2. Dispersion relations of electronic surface states on the clean C(110) surface. Surface states are represented by filled circles, the three different degrees of shading indicate that the states are localized to more than 70%, 80%, and 90% on the upper two surface layers. Darker shading means stronger localization. The shaded areas represent the bulk bands projected with 11 $\vec{k}_z$ values onto the (2×1) surface Brillouin zone (see Fig. 3). Energies are given relative to the Fermi energy.

choose a (2×1) surface Brillouin zone (SBZ) to make it easier to compare to the band structure of the other diamond surfaces and also to other calculations, although the clean C(110) surface shows no reconstruction. The SBZ's of the (1×1) and (2×1) cells can be seen in Fig. 3.

The dangling bonds lead to two bands, which are situated within the bulk gap. Along $\overline{\Gamma J}$ the antibonding p_z surface state has a large dispersion of 3.4 eV and crosses the Fermi level shortly before $\overline{J}$. The bonding surface state that has a $pp\pi$ character disperses downward from $\overline{J}$ and merges with the bulk bands half-way along $\overline{\Gamma J}$. The two bands that are both antibonding p_z states are degenerate along $\overline{JK}$ (perpendicular to the surface chains), where they cross the Fermi level in the middle of this line. Rather intense surface states with an only modest bonding-antibonding splitting are found along $\overline{KJ'}$. In Fig. 4 the nature of the surface states at $\overline{J'}$ in the bulk gap is analyzed. The highest occupied state contributes to the bonding of the surface chains (p_z tilted away from the surface normal), whereas the lowest unoccupied state has a $pp\pi^*$ character [see Figs. 4(a) and 4(b), respectively]. The surface state at $\overline{J'}$ and $E=-5.5$ eV is a strong σ bond.

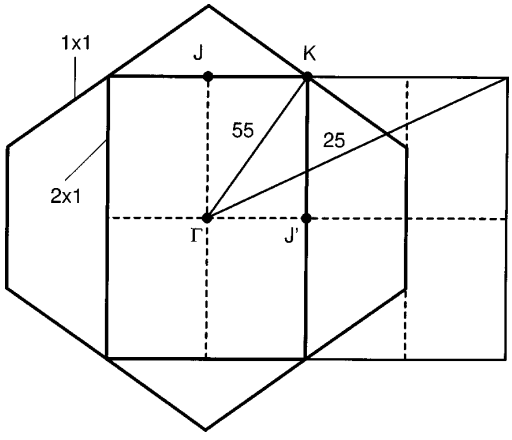

FIG. 3. Surface Brillouin zones of the (1×1) and (2×1) diamond (110) surface.

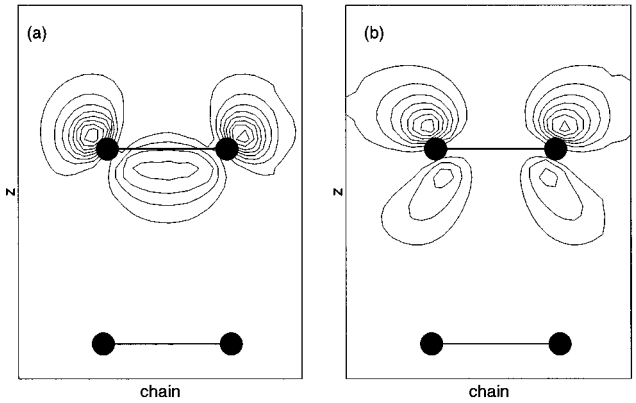

FIG. 4. Charge densities of the clean C(110) surface: (a) highest occupied state at $\overline{J'}$ ($E=-0.5$ eV), (b) lowest unoccupied state at $\overline{J'}$ ($E=0.6$ eV). The densities are shown in a plane perpendicular to the surface and containing one bond of the surface chain. Contour intervals are 0.1 electrons per Å^3 for the partial charge densities.

The surface is metallic, but with a very low density of states at the Fermi level. This can be seen in Fig. 5, where the layer-resolved partial density of states (DOS) for the five top layers of the clean C(110) surface is shown. The surface-related DOS in the gap shows a distinct bonding-antibonding splitting and decreases constantly from the surface to the fifth layer, where only some small features remain. At the valence-band minimum states are removed in the surface layer. For the subsurface layers we find only a relative modest change in the density of states of the valence band.

B. Hydrogenated surface

Hydrogen saturation of the dangling bonds removes the occupied surface states from the gap (see Fig. 6). The surface becomes semiconducting with a direct gap at $\overline{\Gamma}$ of 2 eV. Only around $\overline{J'}$ could we identify a weakly localized occupied surface state split from the valence band; at $\overline{J}$ we find a very weak surface state at $E=-6.2$ eV. Figure 7 shows the charge distribution of the surface state at $\overline{J'}$ and $E=-2.5$ eV. After the saturation of the dangling bonds only a weak $pp\sigma$ bond along the chains remains.

The small intensity of surface states can also be seen in the layer-resolved partial densities of states (Fig. 8). Only in the surface layer we find a certain tendency to a narrowing of the valence band. The empty antibonding states in the gap come practically also only from the first layer.

C. Comparison with photoelectron spectroscopy

To compare with the photoelectron spectra of Francz *et al.*[12] we calculated the local DOS of the first four layers of the clean and the hydrogenated surfaces (i.e., we assume an escape depth of the photoelectrons corresponding to four lay-

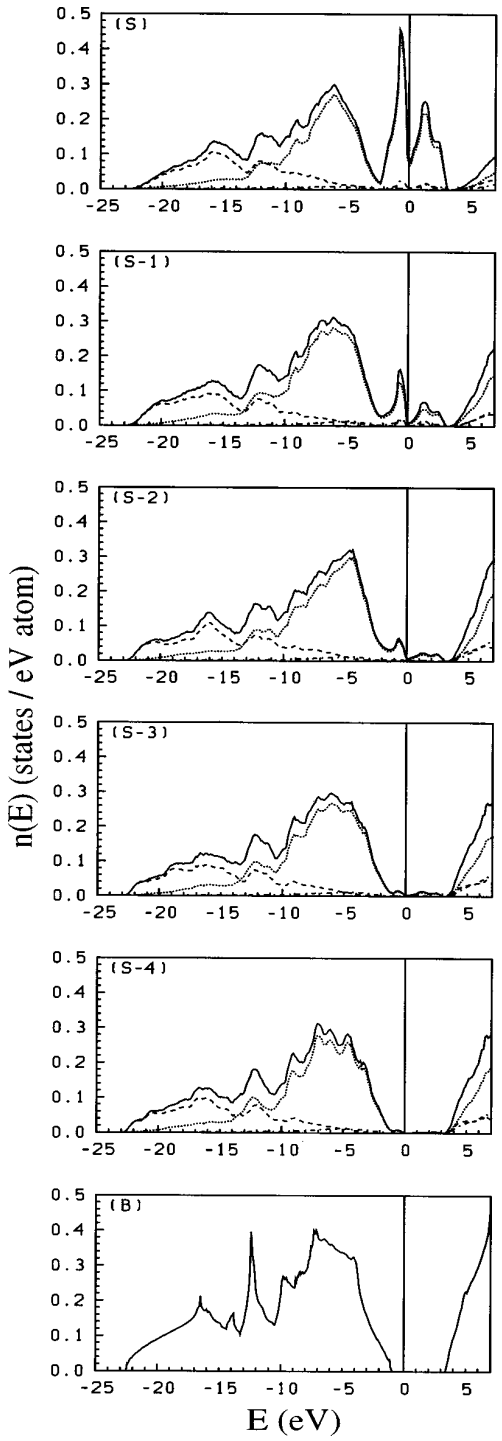

FIG. 5. Layer-resolved total and partial (angular-momentum decomposed) electronic density of states of the clean C(110) surface. S stands for the surface layer, $S1$, $S2$, etc. for the subsurface layers. The density of states of bulk diamond (B) (calculated with $15\times15\times15$ $\vec{k}$ points and a primitive diamond cell) is shown for comparison. Full line: total DOS; dashed, dotted, and dash-dotted lines: s, p, and d DOS, respectively. The energy is measured relative to the Fermi level.

ers). The spectra are aligned such that the position of the peak close to 11.6 eV binding energy characteristic for the sp^3-like bulk DOS agrees for the clean and hydrogenated samples. Energies are measured relative to the VBM of the hydrogen-saturated surface. Figure 9 shows that the clean

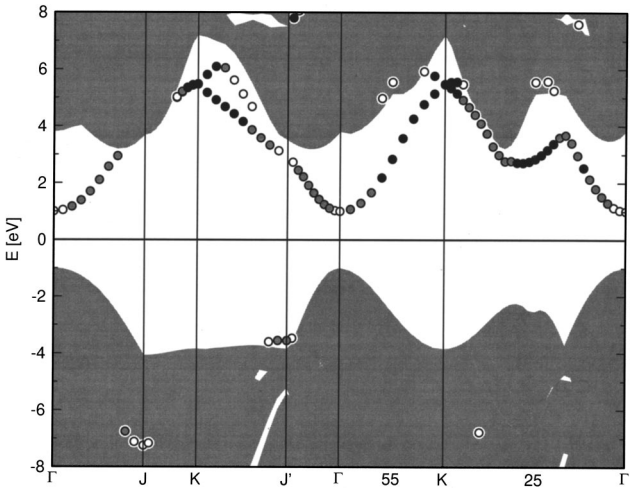

FIG. 6. Dispersion relations of electronic surface states on the C(110):H surface. Cf. Fig. 2.

surface has a higher intensity between the Fermi energy of the clean surface at $E=0.5$ eV (the Fermi energy of the hydrogenated surface lies in the middle of the gap at $E=1.0$ eV) and $E=-1.0$ eV. This intensity comes from the surface states in the bulk gap. From $E=-1.0$ eV down to the first peak of the DOS at $E=-5$ eV the intensity of the hydrogenated surface lies higher than the one of the clean surface. At higher binding energy both intensities are almost identical. This is in good agreement with the theoretical as well as experimental results for the other diamond surfaces: the surface related intensity is concentrated close to the Fermi level for the clean surface and shifted to binding energies of -2 to -7 eV upon hydrogenation, while the

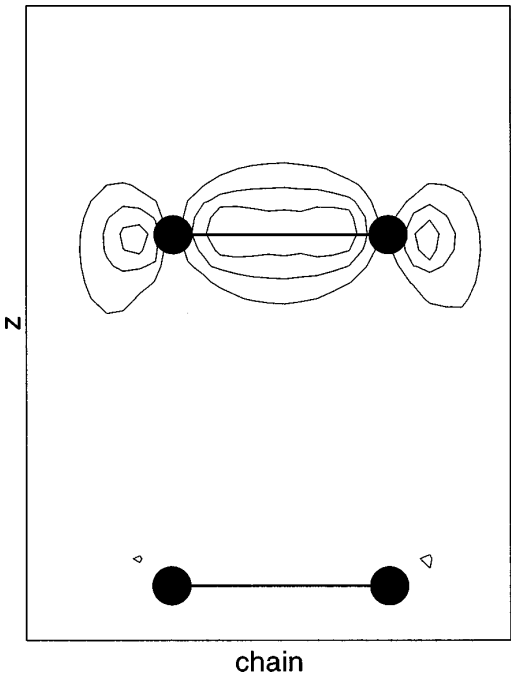

FIG. 7. Charge distribution of the surface state at $\overline{J'}$ ($E=-2.5$ eV) for the C(110):H surface. The density is shown in a plane perpendicular to the surface and containing one bond of the surface chain. Contour intervals are 0.1 electrons per Å^3 for the partial charge density.

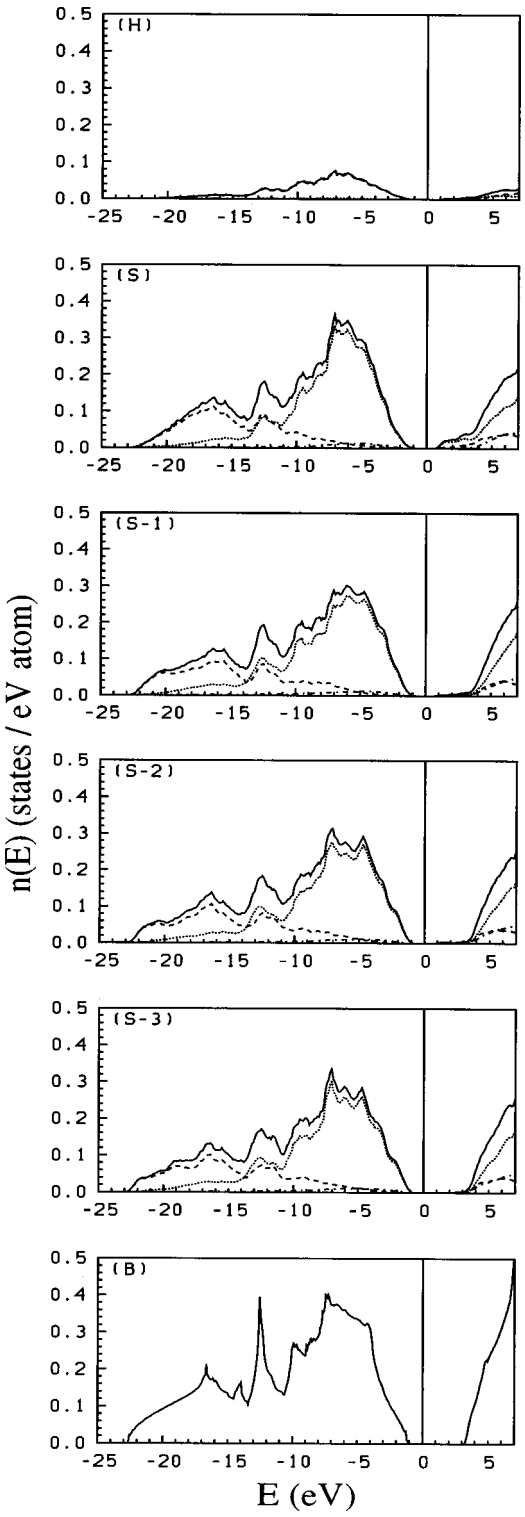

FIG. 8. Layer-resolved total and partial (angular-momentum decomposed) electronic density of states of the C(110):H surface. Cf. Fig. 5.

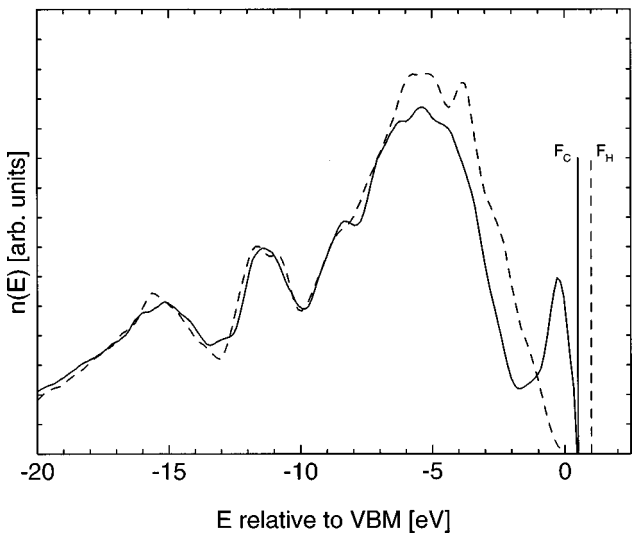

FIG. 9. Total electronic density of states in the top four layers of a clean (full line) and a hydrogenated (dashed line) C(110) surface relative to the valence-band maximum. The positions of the Fermi levels are indicated by the letters F_C and F_H for the clean and the hydrogenated surfaces, respectively. Cf. text.

deeper lying states are essentially bulklike and unaffected by the surface coverage (cf. Refs. 2, 4, and 5). These results are, however, in contrast to the experiments of Francz *et al.*,[12] which showed an increase of the photoemission intensity around -3 and -13 eV below the VBM after annealing (i.e., dehydrogenation) of the C(110) surface. The peak at -3 eV would suggest that the surface states associated with the dangling bonds are located at higher binding energy. A possible explanation of the shift could be a broken symmetry on the clean surface (e.g., dimerization or buckling). Since our self-consistent calculations show that the ideally flat (110) surface has a (1×1) structure such reconstructions [which were also not seen in LEED (Ref. 8)] could be due to imperfections of the surface, such as roughness, defects, and steps. An alternative explanation could be that electronic many-particle effects lift the degeneracy of the surface states along $\overline{JK}$ and lead to an increased bonding-antibonding splitting throughout the entire surface Brillouin zone. Similar effects have been discussed for the C(111) surface.[4] However, the work of Kress, Fiedler, and Bechstedt[32] shows that current many-particle theories predict consistently smaller surface gaps than observed experimentally. For the C(110) surface the quasiparticle gap would have to be even larger to achieve agreement with the data of Francz *et al.*[12]

Another intriguing feature is the strong variation of the DOS at higher binding energies induced by the annealing, which was not reported for the other low-index surfaces. The peak at -13 eV is close to the energetic position of the π states of graphite. However, a possible graphitization of the surface was called in question by Francz *et al.*[12] Our calculations also show no evidence for surface-induced states at this energy on the clean surface. Further investigations are needed to clarify the discrepancies between theory and experiment in the photoelectron spectra.

D. Negative electron affinity

The electron affinity is defined as the energy required to remove an electron from the conduction-band minimum to a distance far away from the surface. Hence it is the energy difference between the vacuum level and the conduction-band minimum. If the vacuum level lies below the conduction-band minimum, no energy barrier prevents low-energy electrons from escaping into the vacuum. In this case

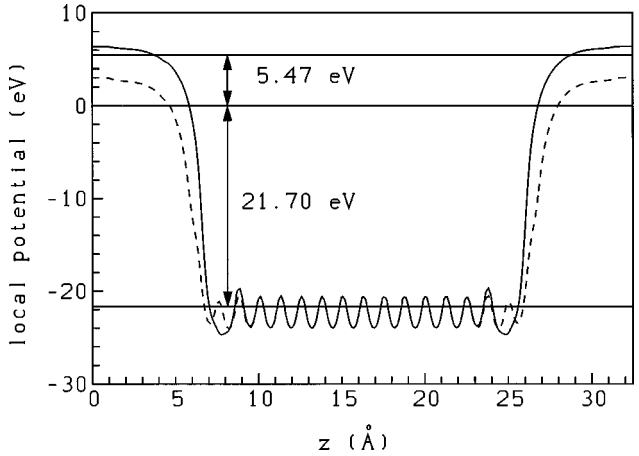

FIG. 10. Calculated plane-averaged self-consistent potentials for the clean C(110) (full line) and the hydrogen-covered C(110):H (broken line) surfaces. The positions of the valence-band minimum and of the conduction-band minimum relative to the valence-band maximum are indicated.

the surface has a negative electron affinity (NEA). Nemanich, Baumann, and van der Weide[13] showed that hydrogen termination can induce NEA on all low-index diamond surfaces, whereas clean or oxygen-terminated surfaces exhibit a positive electron affinity (PEA). We have been able to show that *ab initio* calculations (properly corrected for the error in the LDF gap) allow for a correct prediction of the NEA on C(100) (Ref. 2) and on C(111).[4] Our results for the plane-averaged self-consistent potential along the [110] direction through the relaxed clean and hydrogenated slabs are shown in Fig. 10. For these calculations we used slabs with 10 layers of vacuum to get a better convergence of the potential in the vacuum region. Relative to the valence-band maximum we mark the valence- and conduction-band minima. However, we have to use the experimental value for the optical gap of 5.47 eV and not the too low LDF prediction. This is legitimate because the self-consistent potential depends only on the ground-state properties, which are correctly treated within the LDF. We find a pronounced NEA of 2.4 eV for the hydrogen saturated C(110) surface, whereas the clean surface exhibit a PEA of 0.9 eV. The difference has to be attributed to the lowering of the potential barrier at the surface by the weaker dipole layer on the hydrogenated surface. This comes from the saturation of the dangling bonds with hydrogen. Compared to the (100):H and (111):H surfaces, the hydrogenated (110) shows the largest NEA of the low-index diamond surfaces. All three low-index surfaces have in common that the clean surfaces exhibits a PEA and after hydrogenation they develop a NEA. This is in perfect agreement with the experiments of Nemanich, Baumann, and van der Weide.[13]

VI. DISCUSSION AND CONCLUSIONS

This paper completes our investigations of the structural and electronic properties of the low-index surfaces of diamond. Table III compiles the results for the surface, relaxation, adsorption, etc. energies. The C(110) surface has the lowest cleavage energy. On the C(111) 1db surface where also only one bond per surface atom has to be broken, the cleavage energy is 0.66 eV higher. This shows that, as already emphasized in Ref. 5, simple bond-scission arguments are not appropriate for a reliable estimation of the cleavage energies. For the 1db C(111) and C(110) even a simple relaxation of the surface layer reduces the surface energy by an important amount, whereas for the multiple-dangling surfaces a relaxation is energetically quite ineffective. A reconstruction reduces the energies of the C(100) and C(111) surfaces by almost 50% so that finally the reconstructed C(111) 1db surface has the lowest energy and that the C(100) 2db surface is only 0.46 eV/atom higher in energy than the C(110) surface (which is stable in an unreconstructed state), in spite of a much larger cleavage energy.

Hydrogen adsorption energies are sufficiently higher on all three surfaces to allow for a dissociative adsorption of molecular hydrogen. However, the potential-energy surface for the dissociative adsorption remains to be explored. Unlike for many metallic surfaces, the adsorbate-induced reconstruction (or rather dereconstruction) cannot be neglected for the diamond surfaces — with the exception of the C(110) surface.

TABLE III. Energetics of the low-index diamond surfaces (in eV per surface site). E_{surf} refers to the absolute surface energy. E_{rel} is the relaxation energy relative to the cleavage energy. The number of dangling bonds (db) is indicated.

Structure	C(110) 1db		C(100) 2db [a]		C(111) 1db [b]		C(111) 3db [c]	
	E_{surf}	E_{rel}	E_{surf}	E_{rel}	E_{surf}	E_{rel}	E_{surf}	E_{rel}
(1×1) ideal	2.09		3.89		2.75		4.65	
(1×1) relaxed	1.66	−0.43	3.63	−0.26	2.18	−0.57	4.63	−0.02
(2×1) reconstructed			2.12	−1.77	1.35	−1.40	2.69	−1.96
Hydrogenated	−2.68	−4.77	−2.42	−6.31	−2.80	−5.55	−2.40	−7.05
H adsorption energy [d]	−4.34		−4.54		−4.15		−5.10	
structure of H surface	(1×1):H		(2×1):H		(1×1):H		(2×1):H	

[a]From Ref. 2.
[b]From Ref. 4.
[c]From Ref. 5.
[d]The H adsorption energy is defined as the energy difference between the hydrogenated surface and the stable clean surface.

The governing principle of the reconstruction of all three surfaces is the saturation of the dangling bonds. On the C(100) surface this is achieved by the formation of rows of π-bonded dimers with a bond length of $d=1.37$ Å comparable to that of a C=C double bond in a hydrocarbon molecule. On the C(110) and C(111) (both 1db and 3db) this leads to the formation of π-bonded chains with bond lengths of $d\sim 1.43$ Å comparable to those in graphite. The important difference is that for the C(110) surface chain formation is compatible with the topology of the underlying lattice, whereas on the C(111) surface the six-ring topology of the ideal diamond structure has to be replaced by alternating five- and seven-membered rings.[4,5]

The electronic properties of all three surfaces are characterized by the existence of dangling-bond surface states in the bulk gap and their saturation (or partly saturation) by hydrogenation. For the clean surfaces metallic behavior is predicted for the C(110) and C(111), but not on the C(100) surface.[2] For the C(111) surface electron energy-loss spectroscopy experiments[33] demonstrate the existence of a surface gap of 1 to 2 eV; for the C(110) surface no investigations of the empty surface states have been reported, but the agreement between theory and the available photoemission data could only be improved by a larger bonding-antibonding splitting of the surface states. However, it appears that current quasiparticle theories cannot predict gaps of a width suggested by the experimental data.

ACKNOWLEDGMENTS

This work has been supported by the Austrian Science Foundation with the trinational (Germany-Austria-Swiss) cooperations ''D–A–CH'' on the ''Synthesis of Superhard Materials,'' Project. No S5908-PHYS.

[1] J. Furthmüller, J. Hafner, and G. Kresse, Europhys. Lett. **28**, 659 (1994).
[2] J. Furthmüller, J. Hafner, and G. Kresse, Phys. Rev. B **53**, 7334 (1996) and further references cited therein.
[3] M. Winn, M. Rassinger, and J. Hafner, Phys. Rev. B **55**, 5364 (1997).
[4] G. Kern, J. Hafner, and G. Kresse, Surf. Sci. **366**, 445 (1996).
[5] G. Kern, J. Hafner, and G. Kresse, Surf. Sci. **366**, 464 (1996).
[6] G. Kern, J. Hafner, and G. Kresse, Surf. Sci. (to be published).
[7] K. E. Spear, and M. Frenklach, Pure Appl. Chem. **66**, 1773 (1994).
[8] P. G. Lurie and J. M. Wilson, Surf. Sci. **65**, 435 (1977).
[9] B. B. Pate, Surf. Sci. **165**, 83 (1986).
[10] S. V. Pepper, J. Vac. Sci. Technol. **20**, 213 (1982).
[11] M. McGonigal, J. N. RussellJr., P. E. Pehrsson, H. G. Maguire, and J. E. Butler, J. Appl. Phys. **77**, 4049 (1995).
[12] G. Francz, P. Kania, G. Gantner, H. Stupp, and P. Oelhafen, Phys. Status Solidi B **154**, 91 (1996).
[13] R. J. Nemanich, P. K. Baumann, and J. van der Weide, in *Applications of Diamond Films and Related Materials*, edited by A. Feldman, Y. Tzeng, W. A. Yarbrough, M. Yoshikawa, and M. Murakawa (NIST, Gaithersburg, MD, 1995), pp. 17–24.
[14] B. N. Davidson and W. E. Pickett, Phys. Rev. B **49**, 11 253 (1994).
[15] D. R. Alfonso, D. A. Drabold, and S. E. Ulloa, Phys. Rev. B **51**, 14 669 (1995).
[16] G. Kresse and J. Hafner, Phys. Rev. B **47**, 558 (1993); **49**, 14 251 (1994).
[17] G. Kresse and J. Furthmüller, Comput. Mater. Sci. **6**, 15 (1996).
[18] W. Kohn and L. J. Sham, Phys. Rev. **140**, A1133 (1965).
[19] N. D. Mermin, Phys. Rev. **140**, A1141 (1965).
[20] J. P. Perdew and A. Zunger, Phys. Rev. B **23**, 5048 (1981).
[21] D. M. Wood and A. Zunger, J. Phys. A **18**, 1343 (1985).
[22] P. Pulay, Chem. Phys. Lett. **73**, 393 (1980).
[23] D. Vanderbilt, Phys. Rev. B **41**, 7892 (1990).
[24] G. Kresse and J. Hafner, J. Phys. Condens. Matter **6**, 8245 (1994).
[25] R. D. King-Smith, M. C. Payne, and J. S. Lin, Phys. Rev. B **44**, 13 063 (1991).
[26] J. Furthmüller, J. Hafner, and G. Kresse, Phys. Rev. B **50**, 15 506 (1994).
[27] H. J. Monkhorst and J. D. Pack, Phys. Rev. B **13**, 5188 (1976).
[28] M. Methfessel and A. Paxton, Phys. Rev. B **40**, 3616 (1989).
[29] O. Jepsen and O. K. Andersen, Solid State Commun. **9**, 1763 (1971).
[30] P. E. Blöchl, O. Jepsen, and O. K. Andersen, Phys. Rev. B **49**, 16 223 (1994).
[31] A. Eichler, J. Hafner, J. Furthmüller, and G. Kresse, Surf. Sci. **346**, 300 (1996).
[32] C. Kress, M. Fiedler, and F. Bechstedt, Europhys. Lett. **28**, 443 (1994).
[33] S. V. Pepper, Surf. Sci. **123**, 47 (1983).